ADVANCED ENERGY & SUSTAINABILITY RESEARCH
www.advenergysustres.com

Perovskite-CIGSe Tandem Solar Cell: Over One Year of Outdoor Monitoring

Guillermo Farias-Basulto, Ivona Kafedjiska, Tobias Bertram, Maximilian Riedel, Quiterie Emery, Marko Remec, Paolo Graniero, Mark Khenkin, Christian A. Kaufmann, Iver Lauermann, Reiner Klenk, Rutger Schlatmann, and Carolin Ulbrich*

Tandem solar cells can surpass the limitations of single-junction devices, promising increased performance due to lower thermalization losses. Even though many research and industrial upscaling efforts are based on perovskite-Si tandems, all-thin-film photovoltaic (PV) devices, for instance with chalcopyrite (CIGSe) and perovskite, can offer many advantages such as significant cost and material savings and access to niche markets like building integrated- and flexible PV. However, long-term stability and outdoor performance of perovskite-based tandem devices is to this day challenging. This work presents the first data analysis of year-round outdoor measurements (mpp-tracked) of a perovskite-chalcopyrite tandem device with a starting efficiency of about 23.14% before encapsulation. The maximum outdoor performance of the tandem device changed during the period of observation, reaching the peak performance in April and then decreased due to the device degradation. At its maximum outdoor performance, the tandem could reach up to 68% higher instantaneous power output, relative to its single-junction reference (CIGSe-SJ). In addition, a quantitative time series performance analysis, exemplary qualitative imaging characterization of the tandem before and after outdoor exposure, is shown. Finally, the possibility of predicting the immediate performance of an all-thin-film tandem is verified by using a multiple linear regression model with accuracies generally exceeding 90%.

1. Introduction

The significant increase in photovoltaic (PV) power conversion efficiency (PCE) of perovskite-based PV devices within the last decade has gathered significant attention due to its potential inclusion in a single-junction (SJ) silicon-dominated market.[1]

Perovskite solar cells have already demonstrated a striking and continuously improving record PCE of about 27%.[2,3] Halide perovskites can be fabricated through a broad range of manufacturing options at relatively low deposition temperatures, using abundant materials and lower energy payback time.[4–6] Due to the bandgap tunability, perovskite materials are suitable candidates for tandem devices. In combination with established Si technology, perovskite tandem devices have reached the record PCE above 34%[7] surpassing the Shockley–Queisser limit for SJ solar cells due to the lower thermalization losses.[8,9] These advantages have focused the attention of current development of PV on perovskite-containing tandem devices.[10]

Thin-film tandems, such as perovskite/$Cu(In,Ga)Se_2$ (i.e., CIGSe), offer alternative solutions for niche markets including building integrated PVs or space applications,[11] which require lightweight, flexible, or radiation resistant solar cells.[12,13] However, to be able to penetrate the PV market, perovskite-based PV needs to be commercialized, which can only be done by simultaneously meeting the targets of high efficiency, scalability, and long-term stability.[10,14]

To this day, the highest efficiency achieved for an all-thin-film 2 terminal perovskite-CIGSe tandem is 27.35%,[2,7,15] but to the best of our knowledge, no long-term outdoor stability

G. Farias-Basulto, I. Kafedjiska, T. Bertram, M. Riedel, Q. Emery, M. Remec, P. Graniero, M. Khenkin, C. A. Kaufmann, I. Lauermann, R. Klenk, R. Schlatmann, C. Ulbrich
PVcomB/ Helmholtz-Zentrum Berlin für Materialien und Energie GmbH
Schwarzschildstr.3, D-12489 Berlin, Germany
E-mail: guillermo.farias@helmholtz-berlin.de

The ORCID identification number(s) for the author(s) of this article can be found under https://doi.org/10.1002/aesr.202500162.

DOI: 10.1002/aesr.202500162

G. Farias-Basulto, I. Kafedjiska, T. Bertram, M. Riedel, Q. Emery, P. Graniero, M. Khenkin, C. A. Kaufmann, I. Lauermann, R. Klenk, R. Schlatmann, C. Ulbrich
Helmholtz-Zentrum Berlin für Materialien und Energie
Hahn-Meitner-Platz 1, 14109 Berlin, Germany

M. Remec
University of Ljubljana- Faculty of Electrical Engineering
Tržaška 25, 1000 Ljubljana, Slovenia

R. Schlatmann
HTW Berlin - University of Applied Sciences
Wilhelminenhofstr. 75a, D-12459 Berlin, Germany

measurements have been performed on this type of devices. Until recently, many research endeavors have been put into optimizing the 2 T stack and especially the hole-transport layer (HTL)-perovskite interface so that CIGSe absorbers with varying bandgaps and roughness can be used.[16] Optimizing the interfaces in 2 T perovskite-CIGSe tandem solar cells has shown that using HTL bilayer of copper-doped nickel oxide and a self-assembled molecular monolayer (NiOx:Cu + self-assembled monolayer [SAM]) can lead to satisfactory interfacial charge-carrier dynamics and result in negligible quasi-Fermi level splitting to Voc offset.[17] However, for both SJ perovskite cells and their 2 T tandems with silicon, it was shown that interface modification can have significant implications on the device stability, which has so far not been investigated on the perovskite-CIGSe tandems.[18]

Outdoor-performance and long-term stability measurements of 2 T perovskite-CIGSe solar cells are not yet publicly available, resulting in a profound lack of knowledge not only about their commercialization prospects but also about their degradation pathways.

Motivated by both the progress and the research gap in the field, in this work, we address the stability of an all-thin-film perovskite-CIGSe tandem cell with an initial efficiency of 23.14% and with NiOx:Cu + SAM as HTL. We first discuss the results of maximum power point (MPP) tracking (MPPT) of an encapsulated perovskite-CIGSe tandem outdoors over a period of thirteen months exposed on the rooftop test field in Berlin, Germany. Then we evaluate the data via a machine learning algorithm to extract empiric coefficients that link PV performance to the irradiance and temperature at the field. These coefficients can then be used for power rating of modules[19] and to calculate the power matrix comparable to the international standard IEC61853-1.[20] Additionally, we also track the outdoor performance of a SJ CIGSe solar cell and use it as a benchmark for the evaluation of the tandem's stability. We will also elaborate on the impact of metastability on the outdoor behavior of a perovskite-CIGS tandem.

Our work sets an important milestone in the field of 2 T perovskite-CIGSe tandems since it simultaneously presents the first year-long outdoor performance tracking and validates a model that one can use to insightfully evaluate the performance of tandems.

2. Experimental Section

2.1. Perovskite-CIGSe Tandem Fabrication

The perovskite-CIGSe tandem solar cell presented in this contribution was fabricated following the baseline process developed in previous studies.[16,21]

2.1.1. Bottom Cell

The bottom CIGSe cell was fabricated on a sodium-containing substrate glass coated with 800 nm of molybdenum (Mo) as back contact. Copper, gallium, and indium were coevaporated, under a selenium atmosphere, onto the substrate using a 3-stage physical vapor deposition (PVD) process, which has been developed and published earlier.[22,23] Afterwards, a layer of cadmium sulfide (CdS) of 60 nm was deposited using a chemical bath deposition followed by a window layer composed of a combination of sputtered undoped zinc oxide (i-ZnO) and aluminum doped zinc oxide (AZO). For the reference CIGSe cells, a top contact grid was deposited using silver evaporation (Ag). For the fabrication of tandems, a thinner layer of AZO was used (i.e. 60 nm instead of 120 nm).

The bottom absorber bandgap extracted from the external quantum efficiency (EQE) of a solar cell from the same batch was about 1.08 eV. The bottom cell reference, measured under standard test conditions (STC), demonstrated an open-circuit voltage (*Voc*) of 610 mV and a short-circuit current (*Isc*) of 38 mA cm^{-2}.

2.1.2. Top Cell

The top perovskite cell incorporated a combined HTL including a 15-nm-thick nickel oxide (NiOx) layer doped with 2% copper deposited via low-temperature radio-frequency sputtering and a spin coated SAM (MeO-2PACz([2-(3,6-dimethoxy-9Hcarbazol-9-yl)ethyl]phosphonic acid) annealed for 10 min at 100 °C.[16] The perovskite absorber layer was spin coated, using a triple-cation formulation with an expected bandgap (*Eg*) of 1.63 eV (i.e., $Cs_{0.05}(MA_{0.17}FA_{0.83})_{0.95}Pb(I_{0.83}Br_{0.17})_3$).[24] As electron transport layer, a 20-nm-thick buckminsterfullerene (C60) layer was evaporated on top of the perovskite, followed by a 20 nm of tin oxide (SnOx) layer coated through atomic layer deposition. A transparent conductive oxide composed of a 100-nm-thick indium-zinc oxide layer was deposited on top of the SnOx using DC sputtering, followed by an evaporated layout-defining silver (Ag) top grid electrode. To improve the optoelectrical performance of the tandem solar cell, an antireflective coating of 100-nm-thick LiF was deposited on top of the finished solar cell. These processing steps of the top cell are described in greater detail in a previous study.[16] **Figure 1** presents an image of the whole stack of materials forming a perovskite-CIGSe tandem solar cell, which was obtained through scanning electron microscopy (SEM).

2.1.3. Preparation for Outdoor Measurements

Using electrically conductive adhesive, ribbons were bonded to the negative electrode (Ag) and to the previously exposed positive electrode (Mo). Then, to protect the device from the impacts of ambient atmosphere (most importantly, humidity), the tandem was encapsulated. The encapsulation process was done using the "COM" variant of reference,[25] where the substrate containing the tandem device was placed between two cover borofloat glasses. Between the cover glasses, sheets of polyolefin (POE) were used to mechanically fix the sample to the glasses and minimize optical losses. Additionally, stripes of butyl with a width of about 15 mm were added to the cover glass edges before the encapsulation process to prevent humidity ingress. The encapsulation process itself was performed at 150 °C for 20 min.

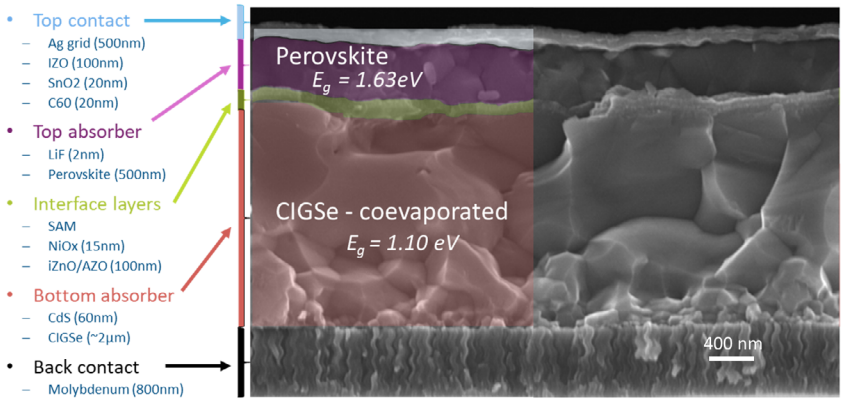

Figure 1. Cross sectional image of a perovskite-CIGSe tandem solar cell before encapsulation obtained through SEM.

2.2. Characterization

2.2.1. Indoor Measurements Techniques

Before encapsulation, the tandem device was characterized using current–voltage (IV) measurements under STC, that is, at 1000 W m^{-2}, 25 °C, and simulated AM 1.5 G spectrum. In this work, we have employed a *Wavelabs* solar simulator equipped with 21 programable LEDs to match the standard spectrum.[20,26] After encapsulation, we have employed a *Wacom* solar simulator with continuous wave illumination using the combined beam of a halogen plus a xenon lamp. JV parameters were extracted from current–voltage measurements under STC.[27,28]

The EQE was measured using the set up and procedure explained in previous publications.[16,21]

Various imaging techniques were employed for quality assurance along different steps of the fabrication process. For photoluminescence (PL) and electroluminescence (EL), a *GreatEyes* system equipped with an InGaAs camera (for the bottom cell) and a Si-camera (for the top cell) was used. For dark lock-in thermography, a setup from *Thermosensorik* equipped with an InSb camera was employed.

2.2.2. Outdoor Measurements

The perovskite-CIGSe tandem was installed at the outdoor test field in Berlin, facing south at an optimal tilt of 35°. The outdoor measurements were performed between the 29th of November 2022 and 31st of December 2023. The device was connected to an MPP tracker provided by the University of Ljubljana (LPVO MP0205M24).[29,30] The device was held at MPP using perturb and observe algorithm. Current and voltage at the MPP (I_{mpp} and V_{mpp}, respectively) were recorded periodically together with environmental parameters.

The global irradiance in plane of array (PoA) was measured using a EKO ML-02 Si-Pyranometer. The device temperature was measured with a digital thermometer (DS18B20) attached to the rear side of the encapsulation.

2.3. Evaluation Algorithms

2.3.1. Multiple Linear Regression (MLR) Model

The machine learning algorithm based on a MLR used in this work has been validated for various applications in SJ PV devices.[31–33] The MLR model is based on a set of equations that describe the behavior of the IV-parameters (e.g., MPP) in relation to PoA irradiance and device temperature. Given that outdoor performance is assessed mainly by the power output of the solar cells, we here limit ourselves to the equation related to the MPP (Equation (1)).

$$MPP_{\mathrm{MLR}} = A_\gamma x_1 + B_\gamma \ln(x_1) x_2 + C_\gamma x_2 + D_\gamma \quad (1)$$

where x_1 represents the irradiance on PoA and x_2 represents device temperature. For devices with high Ohmic losses or semi-ideal behavior, Equation (2) can be used.

$$MPP_{\mathrm{MLR}*} = A_\gamma x_1 + B_\gamma x_1 x_2 + C_\gamma x_2 + D_\gamma \quad (2)$$

After fitting the model to the dataset through error minimization, four coefficients can be extracted. These coefficients are linked specifically to the PV device and its irradiance-temperature-dependent MPP during a specific period. Therefore, it can be used for power rating of modules[19] and to calculate the power matrix comparable to the international standard IEC61853-1.[20]

Generally, the Levenberg–Marquardt algorithm was used for error minimization during the fitting process. For the online implementation of the model, the root mean square error (RMSE) minimization process was used.

3. Results

3.1. Perovskite-CIGSe Tandem

3.1.1. Performance after Fabrication

After fabrication, the JV curve of perovskite-CIGSe tandem was measured multiple times to evaluate performance changes under

STC at specific stages of its lifetime. These measurements were conducted immediately after fabrication and contacting, before encapsulation and after encapsulation.

The initial STC performance of our tandem device was achieved after fabrication (i.e. 23.14%) as illustrated in **Figure 2**A. For comparison, a SJ CIGSe solar cell (bottom cell) reference from the same PVD process achieved an efficiency in SJ of 15.9%, with a PCE of 14.5% after encapsulation.

Figure 2B presents the EQE measured from a representative tandem solar cell using the same fabrication process as the outdoor-installed cell. In this case, the EQE shows a slightly higher current than the one presented by our outdoor tested tandem with a current mismatch of only 0.4 mA cm^{-2}, being slightly bottom cell limited. The apparent bandgap (E_g) obtained from the derivative of both curves equals 1.63 and 1.088 eV for the top and bottom cell, respectively. As expected, the bandgap of the bottom cell of the tandem is consistent with the bandgap obtained from a CIGSe-SJ reference (see Supporting Information A3).

Encapsulation of the tandem using vacuum lamination resulted in relatively high performance-losses. The measurements after encapsulation can be seen in **Figure 3**, where the IV curves after fabrication are shown (black and gray) for comparison. In comparison to the IV-curve measured directly before encapsulation (pink), the first IV-curve measured after encapsulation (red) presented a poor fill factor likely due to a transport barrier formation during the encapsulation process. Notably, a significantly improved performance of the encapsulated device was observed after 1 min of light-soaking under 1-sun spectrum illumination (green), relaxing back to an intermediate state (purple) after a few minutes in the dark. To investigate the origin of the transport barrier, 1 min of light-soaking was used again while placing a long-pass 750 nm filter on top of the sample, which allows only the illumination of the bottom cell. Interestingly, no influence of the light-soaking was then seen (dashed light purple). Afterwards, the filter on top of the sample was removed to light-soak for one more minute resulting in a similar curve as the first one-minute light-soaking (dashed yellow). Thus, the transport barrier causing nonexponential behavior was successfully

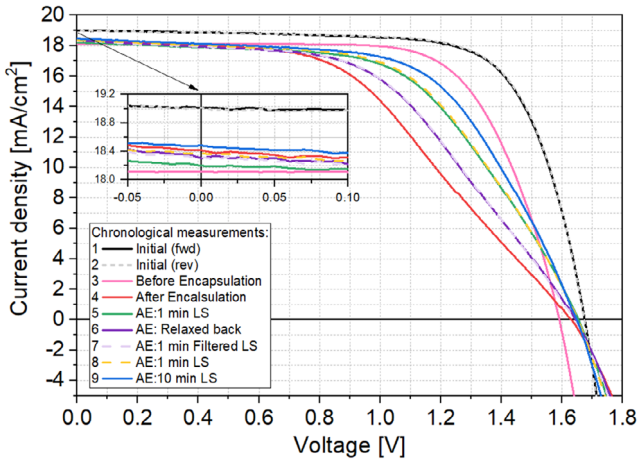

Figure 3. JV curves measured indoors under STC of the perovskite-CIGSe tandem before and after encapsulation, showing reversible metastable behavior revealed by light-soaking.

removed by the application of an unfiltered light-soak, suggesting that the barrier was generated within the top cell. For the last measured IV-curve before outdoor installation (blue), the sample was preconditioned by 10-minute light-soaking, resulting in a PCE of 18.5%.

The improvement of device performance though light soaking has been reported for various PV technologies,[34–36] being especially pronounced in perovskite-based solar cells.[37,38] It was recently shown to have a significant impact on outdoor operation in SJ PSCs and perovskite/Si tandems due to the diurnal cycle of illumination.[29] Therefore, it is not unexpected to observe light soaking effects in perovskite-CIGS tandem cells. The underling mechanistic explanation is still debated[37] and like depends on the device architecture. Possible origins include mobile ions redistribution,[37,39,40] strain relaxation in the perovskite lattice,[41–43] defect healing,[44,45] and charge carriers trapping/detrapping.[39,46] Thus, the stability and durability of perovskite-based solar cells are still being broadly investigated.

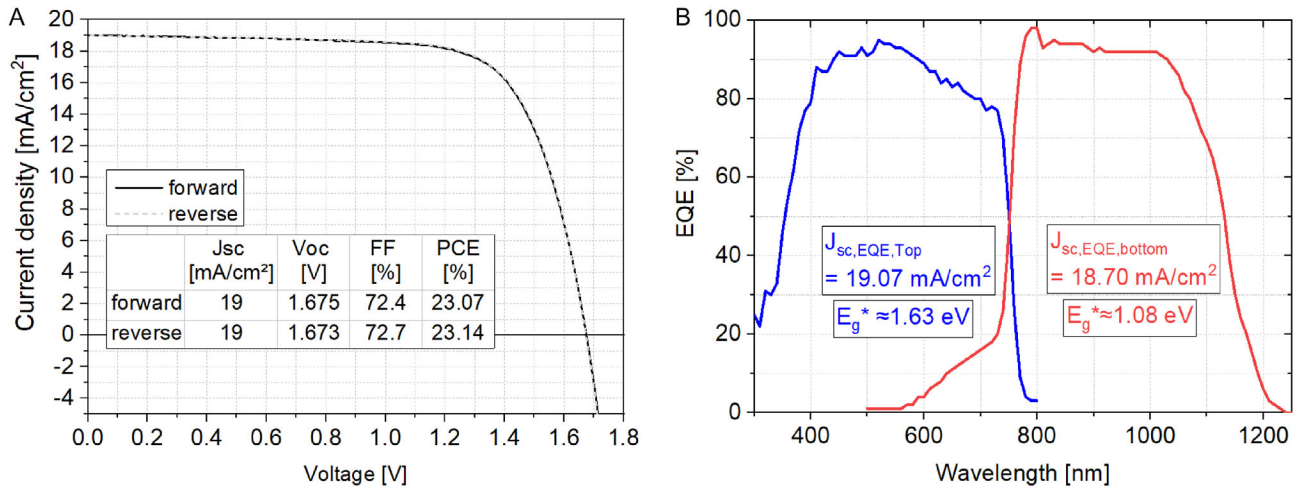

Figure 2. Performance of the unencapsulated CIGS/perovskite tandem after fabrication. A) JV curve and parameters, and B) EQE of a similar device.

3.1.2. Perovskite-CIGSe Tandem Outdoor Performance

The outdoor MPP dataset from the all-thin-film perovskite-CIGSe tandem solar cell comprised in this study contains about 769 000 datapoints measured above 50 W m^{-2} illumination between the 24th of November 2022 and the 31st of December 2023 (data available[47]). Due to a major problem with the data gathering system (after a hack attack), a gap of data is present in our analysis from June 9th to August 4th, 2023. However, only the data acquisition was affected and not the operation of any of the devices in our set up. During the whole exposure period, including the summer months affected by the attack, the device under study was held outdoors under the MPP condition without interruptions.

During the first week of outdoor operation, the power output of the tandem was considerably below the indoor-measured value. However, the tandem improved considerably during the spring months. To better evaluate the performance of our tandem and to have a point of reference, a SJ CIGSe control cell from a similar process was fabricated using the same processes as the bottom cell and the same layout as the tandem (≈1.08cm^2 active area). Said reference obtained an efficiency indoors after encapsulation of 14.5% (see Supporting Information A3) and was installed outdoors on the 19th of April 2023. For the CIGSe reference cell, a silver top contact with three fingers was used given that the SJ CIGSe generates about twice as much current density as the tandem.

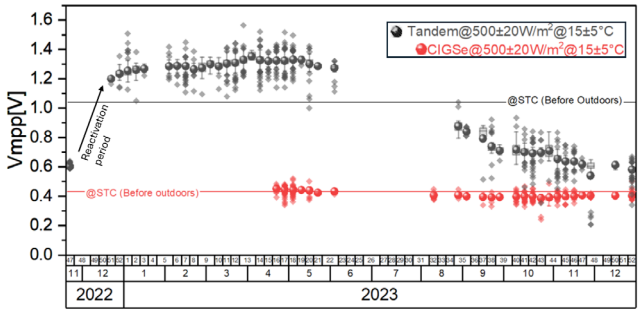

Figure 4. Voltage at MPP during outdoor measurements for a perovskite-CIGSe tandem in comparison to a SJ CIGSe solar cell. Weekly averaged values are shown after filtering the data by 500 ± 20 W m^{-2} and device temperature of 15 ± 5 °C.

Figure 4 shows a comparison of the voltage at the MPP (V_{mpp}) for both the tandem and the CIGSe SJ reference, where the average values per week are shown respectively as solid circles in black and red. As reference, the average measurements of irradiances and cell temperature (back glass) per week performed during 2023 are shown in **Figure 5**. Data points were filtered to include values within a narrow range of irradiance (500 ± 20 W m^{-2}) and temperature (15 ± 5 °C) to ensure meaningful comparisons and for better visualization. A here forth addressed as "reactivation period" can be seen during the first month after installation, going from a low performing device to a tandem working as a tandem. Although on a different timescale, similar to our observation indoors, the "reactivation" implies that the free-carrier transport barrier causing the limiting of voltage at MPP was removed possibly due to light-soak promoted ion migration within the top cell.[37,48] The "reactivation" period was followed by a further increase of the V_{mpp} in summer period. Such behavior was previously reported for perovskite SJ devices.[49] In comparison, the CIGSe SJ cell shows only minor changes in V_{mpp} during the observation period.

Figure 6 presents the MPP data filtered for 1000 ± 10 W m^{-2} and 25 ± 5 °C, where the weekly averaged values are shown as bigger dots. These values (and averages) represent the closest possible values to STC values as a base for comparison as it is very unlikely to find outdoor data matching the exact STC conditions. Ideally, assuming no degradation or metastability, the averaged data should follow a straight line, as it is arguably

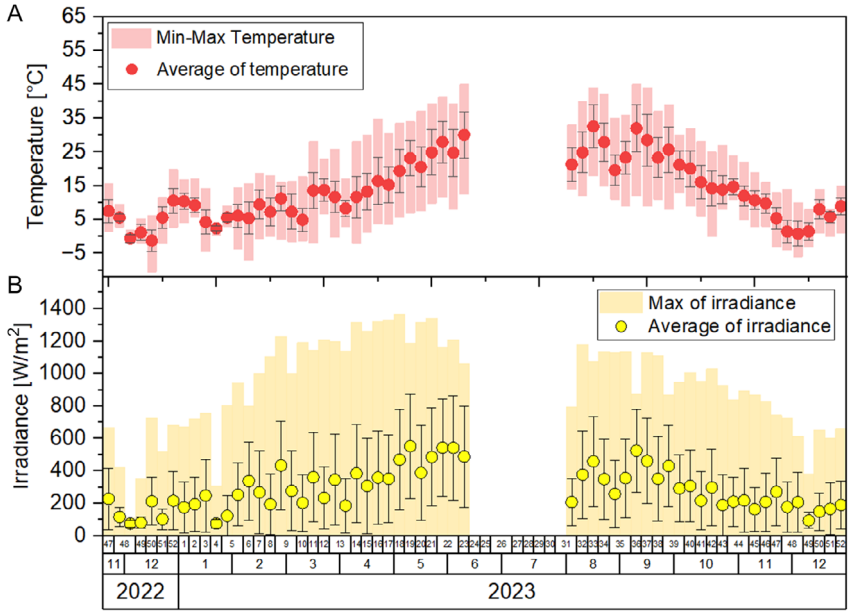

Figure 5. A) Measurements of irradiance and B) cell temperature for each week during 2023.

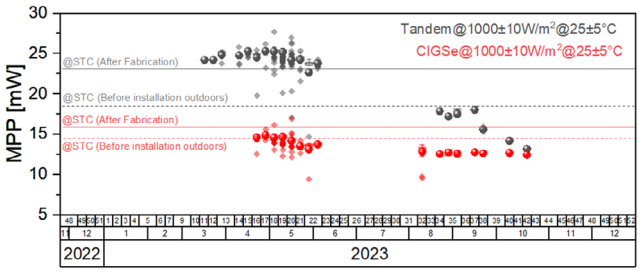

Figure 6. MPP of outdoor measurements of a perovskite-CIGSe tandem and a SJ CIGSe solar cell. Filtered by $1000 \pm 10\,W\,m^{-2}$ and device temperature of 25 ± 5 °C. The values are binned weekly, and the average values are shown with large symbols.

the case for the CIGSe reference (in red) especially after the data gap. Thus, the increase of the MPP beyond even the "after fabrication" value (solid gray line) during the spring months clearly indicates an improvement of performance, achieving a maximum instantaneous power, which on average, exceeded $25\,mW\,cm^{-2}$ under STC conditions.

Similarly to Figure 4, the improvement of the tandem cell can be linked to the metastable behavior seen in its indoor measurement (see Figure 3). As shown in literature for the stated location and angle of installation,[29] the magnitude of global irradiance and exposure time of irradiance increases toward summer due to the increase of the zenith. This increment, together with the increase of temperature and of blue shifted spectra,[50,51] provided an appropriate scenario for the necessary light-soaking needed to passivate the barrier within the top cell, increasing the optoelectrical properties of our tandem.

To assess the performance of our tandem in comparison to a SJ device, we employed the relative gain in MPP of the tandem with respect to the SJ CIGSe. **Figure 7** presents an example of a clear sky day after the installation of the CIGSe reference (red) and the tandem (black). Under peak irradiance conditions ($\approx 1000\,W\,m^{-2}$), the tandem device achieved a total output of around $25\,mW\,cm^{-2}$. The relative gain curve (blue) illustrates the performance advantage of the tandem over the SJ cell under varying operating conditions, obtaining a maximum relative increase in performance of about 68%.

3.1.3. Discussion: Degradation and Light-Soaking Effect

The increase in the relative gain in Figure 7 could suggest a light-soaking effect and/or a current mismatch arising from the differences arising from spectral variations throughout the day. Before the zenith, the relative gain exhibited a positive trend, increasing from ≈27% to 68%. However, after the zenith (Berlin, April 22, 2023, ≈13:04 PM GMT + 2), the trend remained relatively constant, with a slight decrease from 68% to 62%. Thus, while both factors (i.e., light-soaking and current mismatch) could contribute to the observed trend, the relative gain comparison before and after the zenith suggests that the light-soaking effect was the dominant one. Similar curves and behaviors for each month are provided in the supplementary information (Supporting Information A1).

Figure 8 presents outdoor-measured MPP of our perovskite-CIGSe tandem filtered for three irradiances (i.e. 1000, 500, and $200\,W\,m^{-2}$) and temperatures (25, 15, and 10 °C, respectively), where we emphasize the average with a larger symbol. Similarly to Figure 6, ideally, the averaged data should follow a straight-line trend. This is shown by the dashed lines representing, from top to bottom, the STC measurement after fabrication and a fraction of this power by 50% and 20%, assuming a linear decrease of power with irradiance. However, the power increases toward spring, for the 1000 and $500\,W\,m^{-2}$ cases, being particularly more visible at high irradiances. Interestingly, the light-soak

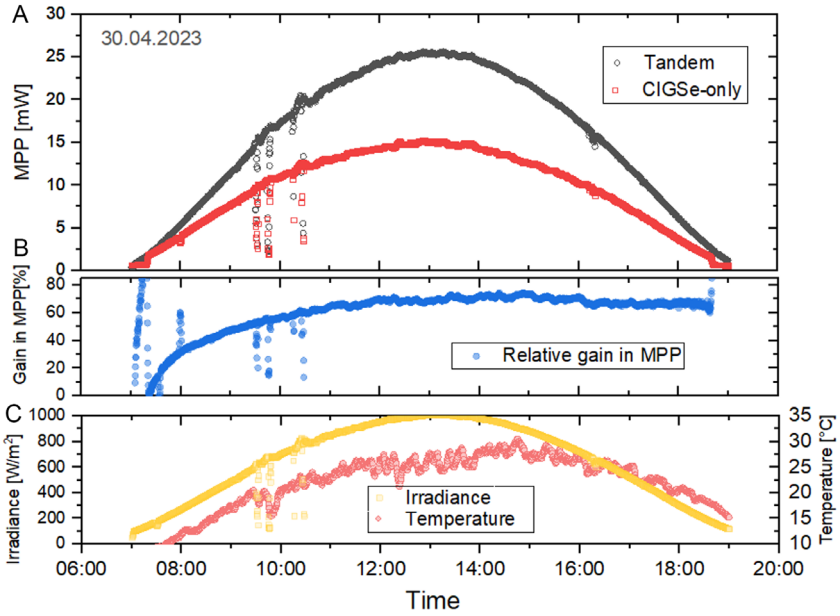

Figure 7. Representative diurnal performance example of our perovskite-CIGSe tandem and a SJ CIGSe reference on a sunny day. A) Instantaneous power. B) Relative gain. C) Measured irradiance and cell temperature.

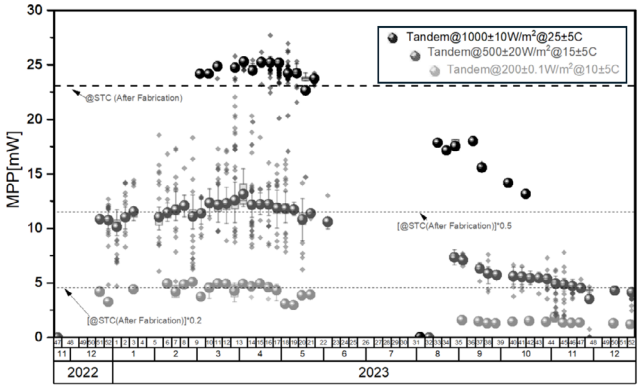

Figure 8. MPP of outdoor measurements for a perovskite-CIGSe tandem filtered for specific irradiances and temperatures.

during the improvement period seems to have a negligible influence on low irradiances. According to the single diode model,[52–54] this discrepancy between high and low irradiances suggests an improvement of the quality of the diode (before maximum performance) and not a particular influence of parasitic resistances. However, the lowering of power at 200 W m^{-2} already by the end of May suggests the beginning of the deterioration starting before summer, followed by a clear decrease in power after/during summer for the three scenarios, being more pronounced for the 1000 W m^{-2} at 25 °C case, where the values measured were reduced below the "after fabrication" limit.

By the end of October 2023, the tandem appears to have no further relative gains, obtaining comparable values to the SJ CIGSe reference which can be seen in Figure 4 and Figure 6. The latter is also supported by a power drop at 500 and 200 W m^{-2} in October with a further decrease in performance, which suggests a degraded tandem.

There are many degradation mechanisms identified in the perovskite-based PV devices,[55,56] some of which are likely to be also present in the CIGSe/perovskite. According to Deng et al.[38] light-soaking during bias voltage causes dynamic processes that promote the accumulation of ions at the interface between perovskite and transport layer, which can have a negative or a positive influence on the device. In our measurements along the year-long monitoring, unknown processes within the top cell were both beneficial and detrimental to V_{mpp} (as in Figure 4). The qualitative PL images of our tandem before and after outdoor measurement presented in **Table 1**, show a clear formation of bubble-like structures within the whole tandem (top and bottom). These structures can be seen in the optical image, found close to the external cathode, indicating delamination. Even though similar defects have been found in literature,[57] the exact reason behind the improvement and bubble formation of the tandem remains an open question for future research.

3.2. MLR Model for Tandem Devices

As previously mentioned, the MLR model has been used to fill data gaps of SJ devices and to extract diode parameters given its strong correlation to the one diode model.[19,31] However, given that the measurements available in this work are based on MPP-tracking and not IV-tracing, the diode parameters cannot be currently extracted with this model. Also, due to the large data gap during which degradation of the device occurred, the data gap filling requires a deeper understanding of MLR coefficients relative to device degradation of the tandem which is beyond the scope of this work. Thus, we emphasize the usability of the MLR in terms of the error of the MLR as a black box model to verify its applicability to perovskite-CIGSe tandem devices.

3.2.1. Verification of Model

To verify the model, we have used data from the month of May given that, during this month, the evaluated tandem was mostly stable. Only data above 200 W m^{-2} was used to reduce the impact of the irradiance sensor uncertainty. **Figure 9** presents the relative error between the measured MPP value and the estimated MPP values calculated using the four coefficients extracted from the fit, where for x_1 and x_2, the measured irradiance and device temperature were respectively used. A relative error lower than 10% was found in almost the whole range of irradiances for the entire period of observations (see the black line in Figure 8), with a total mean relative error of 4.5%. The causes of this considerable error, in addition to the ones found in SJ devices (such as parasitic resistance dominated behavior),[19] can be expected to

Table 1. Qualitative images of a perovskite-CIGSe tandem device before and after outdoor measurements.

PL tandem (Top cell only) (it:300 ms)	PL tandem (Top cell only) (it:250 ms)	PL tandem (Bot cell only) (it:5000 ms)	Photograph tandem
Before outdoors	After outdoors	After outdoors	After outdoors
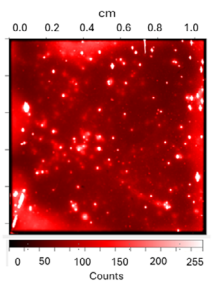	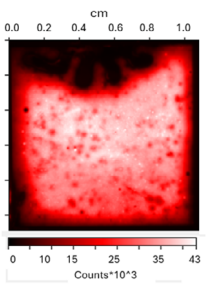		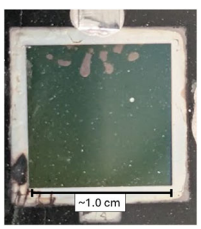

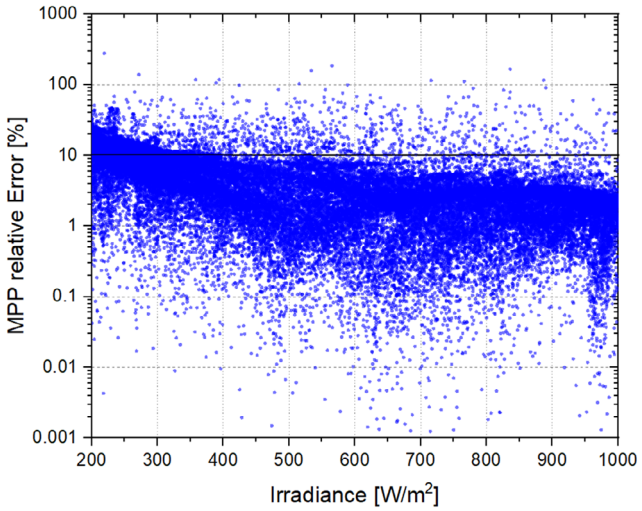

Figure 9. Relative error in estimated MPP by MLR model compared to experimentally measured MPP, shown as a function of irradiance. All datapoints measured in May 2023 were used.

originate from the metastable behavior of the tandem as well as measurements inaccuracies in MPPT, irradiance and temperature, especially during rapid changes in weather conditions (e.g., cloudiness).

Figure 10 shows the comparison of MLR model estimation and the measured power output of the device during a mostly clear sky day, by employing the (mainly) clear sky data presented previously (i.e., Figure 7), which is shown in black. The estimated MLR values are in good agreement with measured data. Figure 10 also shows the relative error in blue, which in comparison to the monthly data, is presented in nonabsolute terms to better visualize the variation of the error throughout the day. For instance, during the highest performance of the cell, the error nears zero, whereas the trend changes before the zenith from negative to positive can be interpreted as an effect of the aforementioned metastable behavior. A mean error of 0.87% was obtained from the absolute error of each value presented in Figure 10. The irradiance valley between at 9 and 10 am represents a "cloudy lapsus", leading to more prominent errors. This points to possible strong changes in the spectrum or difference in the measurement equipment response times that generate mismatched currents within the tandem cell and MPP-tracking inaccuracies.

A value approaching indoor STC can be calculated using the MLR by assuming 1000 W m^{-2} and 25 °C and assuming spectral influences at such higher irradiances can be neglected. Using the extracted coefficients shown in Figure 10, the efficiency of the tandem during the exemplary day equals 25.5%, which agrees with measured values for the same conditions with a relative error below 1%. In addition, the temperature coefficient of the cell can be calculated using the derivative with respect to temperature of Equation (2). In the MLR, the temperature coefficient is a function of irradiance, as expected from literature.[58] By employing the MLR coefficients extracted from clear sky data, the temperature coefficient of the MPP at 1000 W m^{-2} equals −0.063 mW $°C^{-1}$.

3.2.2. Online Machine Learning Optimization

To improve the applicability of the MLR model for real-time outdoor performance assessment, an online learning approach was implemented. Instead of relying solely on a static dataset for model training, the regression coefficients are continuously updated as new measurement data becomes available. This approach is explored in the hope that it may help the model remain responsive to temporal variations in tandem solar cell

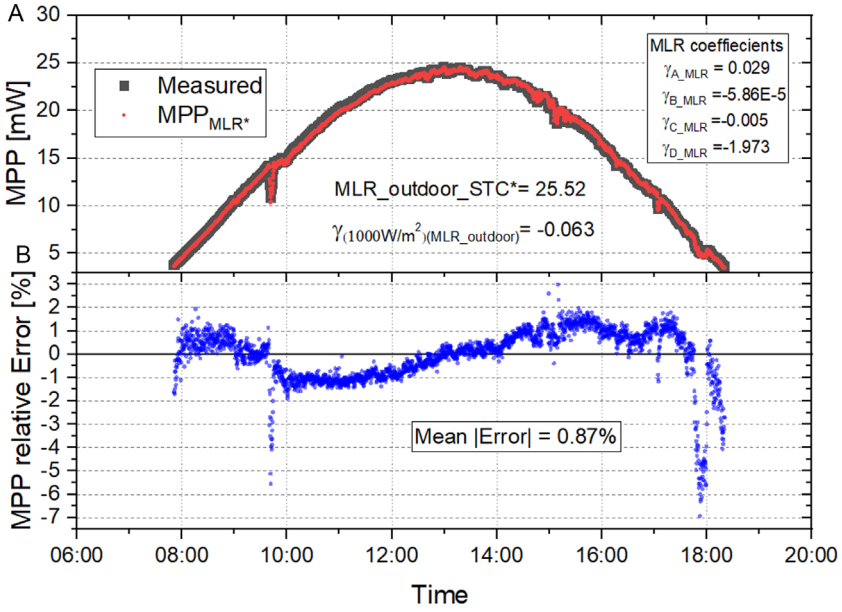

Figure 10. Example of the application of Equation (2) to an all-thin-film perovskite-CIGSe data acquired on the 22nd of April 2023 (see Figure 7). A) Overlap between measured data and recalculated values of MPP. B) Relative error between estimation and measured values of MPP.

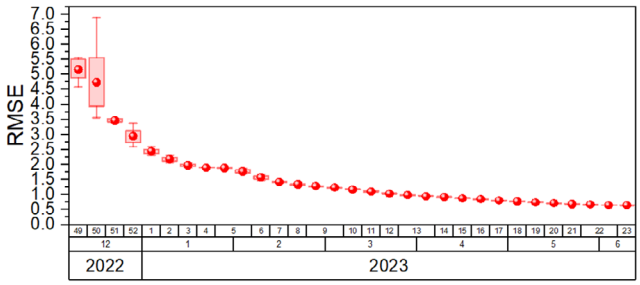

Figure 11. Evolution of the RMSE over time applying the online learning approach to outdoor tandem data.

behavior, particularly considering metastable and degradation effects that could influence performance over time.

The online learning approach allows for incremental updates as new data points are processed. Rather than fitting the model to an entire dataset at once, the regression parameters are adjusted dynamically with each new observation. This enables the model to adapt to changing environmental conditions, such as fluctuations in irradiance and temperature, without requiring complete retraining. By continuously incorporating new information, the model may better reflect real-world performance variations, potentially improving predictions of seasonal efficiency changes, transient light-soaking effects, and degradation patterns.

Additionally, this approach is expected to facilitate continuous error monitoring, ensuring that model predictions remain within an acceptable accuracy range even as environmental conditions fluctuate. The ability to track real-time deviations may provide insights into performance trends, allowing for adjustments and refinements in future implementations.

For this study, data collected from December 2022 to December 2023 was used to evaluate the model's effectiveness in tracking these performance variations over time. The results will provide a foundation for assessing the feasibility of online learning techniques in PV performance modeling and optimization.

Figure 11 illustrates the evolution of the RMSE over time as the online learning approach is applied. Initially, the RMSE is relatively high, reflecting the model's lack of prior knowledge, and the limited amount of training data available in the early stages. However, as new data points are continuously incorporated, the RMSE rapidly decreases, indicating an improvement in model accuracy. By mid-year, the error stabilizes at a consistently low level, suggesting that the model has successfully adapted to the underlying patterns in the data. This trend highlights the effectiveness of the online learning approach in dynamically refining the regression coefficients and reducing prediction errors without requiring full retraining. The sustained low RMSE toward the end of the year indicates that the model remains robust despite seasonal variations and external fluctuations in environmental conditions.

4. Conclusions

This work presented for the first time over one year of outdoor-measured data obtained from a CIGSe/perovskite tandem device. To enable this experiment, a tandem with an initial indoor (STC) performance of 23.1% was encapsulated between two glasses and installed on a test field in Berlin, Germany, where it was measured through MPP-tracking. After encapsulation the device presented a considerable loss in PCE (18.5%), which was proved to be reversible to a certain degree through light soaking. Our filter light soak (long-pass 750 nm) showed no improvement, which indicated to the top cell as major contributor to this improvement. During the outdoor-measurement period, the performance of the tandem improved at first, reaching outdoor PCE values even above those measured indoors, reaching its best performance outdoors in spring (≈25.5%), to later decrease due to device degradation. Layer delamination was found to be one of the major contributing degradation mechanisms. Importantly, we have presented the tandem's diurnal performance behavior in comparison to a SJ CIGSe device during a sunny day, which indeed showed higher real-world outdoor performance as expected. One important difference between the tandem cell and reference bottom cell operation is the metastability, as was previously shown for perovskite SJ and perovskite/Si tandem cells, which may delay their commercialization.

We also demonstrated that MLR models are applicable to satisfactory (accuracy mostly >90%) describe the outdoor behavior of CIGSe/perovskite tandems. Although the errors are not negligible, particularly due to the metastability of the device, the error can be reduced using online machine learning algorithms, and to the best of our knowledge, this work presents the first experimental validation of any energy yield models for this kind of device.

Supporting Information

Supporting Information is available from the Wiley Online Library or from the author.

Acknowledgements

This project is cofunded by the European Union. M.R. and M.K. thank the TAPAS project (Tandem Perovskite And Silicon solar cells—Advanced optoelectrical characterization, modelling and stability) within the EU partnering program (PIE-0015). P.G. gratefully acknowledges funding from the German Federal Ministry of Education and Research (BMBF) for the Solar TAP innovation platform under the Helmholtz Innovation Platforms funding line. The authors also thank HZB-PVcomB staff, especially Tim Münchenberg, Bianka Bunn, and Jakob Lauche for baseline processing, and Stefan Janke and Steven Melendez for PL/EL maintenance and measurements. The authors thank Steve Albrecht and the Hysprint labs for providing the infrastructure for perovskite processing and Eike Körner for the top grid design used on the CIGSe reference.

Conflict of Interest

The authors declare no conflict of interest.

Author Contributions

Guillermo Farias-Basulto: conceptualization (lead); data curation (equal); formal analysis (lead); investigation (lead); methodology (lead); supervision (equal); validation (lead); visualization (lead); writing—original draft (lead); writing—review and editing (lead). **Ivona Kafedjiska**: data curation

(equal); formal analysis (equal); investigation (equal); writing—review and editing (supporting). **Tobias Bertram**: conceptualization (supporting); data curation (supporting); formal analysis (supporting); investigation (supporting); writing—review and editing (supporting). **Maximilian Riedel**: data curation (equal); software (equal). **Quiterie Emery**: data curation (supporting). **Marko Remec**: conceptualization (supporting); data curation (equal); methodology (supporting); software (equal); writing—review and editing (supporting). **Paolo Graniero**: conceptualization (supporting); data curation (supporting); formal analysis (equal); methodology (supporting); software (equal); writing—original draft (supporting). **Mark Khenkin**: validation (equal); writing—review and editing (equal). **Christian A. Kaufmann**: funding acquisition (equal); investigation (equal); project administration (equal); supervision (lead). **Iver Lauermann**: funding acquisition (equal); project administration (equal); resources (equal); supervision (equal). **Reiner Klenk**: funding acquisition (equal); project administration (equal); resources (equal); supervision (equal); validation (equal); writing—review and editing (equal). **Rutger Schlatmann**: funding acquisition (equal); supervision (equal). **Carolin Ulbrich**: conceptualization (equal); funding acquisition (equal); project administration (lead); resources (equal); supervision (equal); validation (equal).

Data Availability Statement

The data that support the findings of this study are openly available in https://doi.org/10.5442/ND000012 at https://doi.org/10.5442/ND000012, reference number 12.

Keywords

$Cu(In,Ga)Se_2$, machine learning, perovskite, solar energy, tandem

Received: April 16, 2025
Revised: July 18, 2025
Published online: August 27, 2025

[1] S. Philipps, "Photovoltaics-Report 2024." Freiburg, Germany: Fraunhofer ISE and Werner Warmuth, PSE Projects GmbH, May 17, **2024**.
[2] "Interactive Best Research-Cell Efficiency Chart | Photovoltaic Research | NREL." (Accessed: Aug, 2025), [Online]. Available: https://www.nrel.gov/pv/interactive-cell-efficiency.html.
[3] Soochow/UNSW/BaimaLake, "World-leading 27% perovskite cell efficiency record set by UNSW and Soochow University, with ACAP support," *ACAP*. (Accessed: Aug, 2025), [Online]. Available: https://www.acap.org.au/post/world-leading-27-perovskite-efficiency-record-achieved-by-unsw-and-soochow-university-with-acap-su.
[4] A. Agresti, F. Di Giacomo, S. Pescetelli, A. Di Carlo, *Nano Energy* **2024**, *122*, 109317.
[5] L. Yuan, Q. Xue, F. Wang, N. Li, G. I. N. Waterhouse, C. J. Brabec, F. Gao, K. Yan, *Chem. Rev.* **2025**, *125*, 5057.
[6] Y. Galagan, *Oxford Open Mater. Sci.* **2021**, *1*, itaa007.
[7] M. A. Green, E. D. Dunlop, M. Yoshita, N. Kopidakis, K. Bothe, G. Siefer, X. Hao, J. Y. Jiang, *Progress in Photovoltaics: Research and Applications* **2025**, *33*, 795.
[8] W. Shockley, H. J. Queisser, *J. Appl. Phys.* **1961**, *32*, 510.
[9] Y. Blom, M. R. Vogt, C. M. Ruiz Tobon, R. Santbergen, M. Zeman, O. Isabella, *Solar RRL* **2023**, *7*, 2200579.
[10] H. Wang, Y. Wang, Z. Xuan, T. Chen, J. Zhang, X. Hao, L. Wu, I. Constantinou, D. Zhao, *Materials* **2021**, *14*, 6569.
[11] N. Albinius, B. Rau, M. Riedel, C. Ulbrich, *Energies* **2025**, *18*, 1293.
[12] C. A. Kaufmann, D. Greiner, S. Harndt, R. Klenk, S. Brunken, R. Schlatmann, M. Nichterwitz, *Flexible Cu(In,Ga)Se2 Thin Film Solar Cells for Space Applications - Recent Results from a German Joint Project (PIPV2)* 5. Amsterdam, The Netherlands, EU PVSEC Proceedings, **2014**. https://doi.org/10.4229/29thEUPVSEC2014-4CV.2.49.
[13] I. Jeong, T. K. Lee, H. V. Tran, I. Hwang, J. Hwang, A. Lee, S. Ham, H. Tran, Y. Cho, D. Shin, S. Song, S. Lee, S. K. Ahn, Y. Eo, A. Cho, J. H. Park, J. Cho, J. Byeon, W. M. Kim, J. H. Yun, J. Gwak, S. Hong, S. Ahn, H. J. Kim, K. Kim, *Joule* **2024**, *9*, 101794.
[14] E. Aydin, T. G. Allen, M. De Bastiani, A. Razzaq, L. Xu, E. Ugur, J. Liu, S. De Wolf, *Science* **2024**, *383*, eadh3849.
[15] F. Pei, S. Lin, Z. Zhang, S. Lin, X. Huang, M. Zhao, J. Xu, X. Zhuang, Y. Zhang, J. Tang, Y. Chen, K. Li, L. Wang, G. Liu, D. Qian, H. Liu, W. Zhou, Y. Chen, J. Wang, H. Zhou, B. Li, D. Zhong, Y. Jiang, Q. Chen, *Nat. Energy* **2025**, *10*, 824–835.
[16] I. Kafedjiska, G. A. Farias-Basulto, P. Reyes-Figueroa, T. Bertram, A. Al-Ashouri, C. A. Kaufmann, R. Wenisch, S. Albrecht, R. Schlatmann, I. Lauermann, *Sol. Energy Mater. Sol. Cells* **2023**, *254*, 112248.
[17] I. Kafedjiska, I. Levine, A. Musiienko, N. Maticiuc, T. Bertram, A. Al-Ashouri, C. A. Kaufmann, S. Albrecht, R. Schlatmann, I. Lauermann, *Adv. Funct. Mater.* **2023**, *33*, 2302924.
[18] S. Mariotti, E. Köhnen, F. Scheler, K. Sveinbjörnsson, L. Zimmermann, M. Piot, F. Yang, B. Li, J. Warby, A. Musiienko, D. Menzel, F. Lang, S. Keßler, I. Levine, D. Mantione, A. Al-Ashouri, M. S. Härtel, K. Xu, A. Cruz, J. Kurpiers, P. Wagner, H. Köbler, J. Li, A. Magomedov, D. Mecerreyes, E. Unger, A. Abate, M. Stolterfoht, B. Stannowski, R. Schlatmann, L. Korte, S. Albrecht, *Science* **2023**, *381*, 63.
[19] G. A. Farias-Basulto, P. Reyes-Figueroa, C. Ulbrich, B. Szyszka, R. Schlatmann, R. Klenk, *37th EU PVSEC* **2020**, *7*, https://doi.org/10.4229/EUPVSEC20202020-3CO.8.3.
[20] IEC, IEC 61853-1:2011, "Photovoltaic (PV) module performance testing and energy rating - Part 1: Irradiance and temperature performance measurements and power rating," **2011**. (Accessed: Aug, 2019). [Online]. Available: https://webstore.iec.ch/publication/6035.
[21] I. Kafedjiska, G. Farias Basulto, F. Ruske, N. Maticiuc, T. Bertram, C. A. Kaufmann, R. Schlatmann, I. Lauermann, *J. Phys. Energy* **2023**, *5*, 025008, https://doi.org/10.1088/2515-7655/acc277.
[22] T. Kodalle, T. Bertram, R. Schlatmann, C. A. Kaufmann, *IEEE J. Photovoltaics* **2019**, *9*, 1839.
[23] T. Kodalle, H. A. Yetkin, A. V. Tovar, T. Bertram, R. Klenk, R. Schlatmann, C. A. Kaufmann, *IEEE J. Photovoltaics* **2021**, *11*, 232.
[24] M. Saliba, T. Matsui, J. Seo, K. Domanski, J. Correa-Baena, M. K. Nazeeruddin, S. M. Zakeeruddin, W. Tress, A. Abate, A. Hagfeldt, M. Grätzel, *Energy Environ. Sci.* **2016**, *9*, 1989.
[25] Q. Emery, M. Remec, G. Paramasivam, S. Janke, J. Dagar, C. Ulbrich, R. Schlatmann, B. Stannowski, E. Unger, M. Khenkin, *ACS Appl. Mater. Interfaces* **2022**, *14*, 5159.
[26] NREL, "Solar Spectral Irradiance: ASTM G-173," The National Renewable Energy Laboratory. (Accessed: Aug, 2020). [Online]. Available: https://www.nrel.gov/grid/solar-resource/spectra-am1.5.html.
[27] J. A. Duffie, W. A. Beckman, *Solar Engineering Of Thermal Processes* Wiley, University of Wisconsin-Madison, **2013**.
[28] T. Markvart, A. McEvoy, L. Castaner, *Practical Handbook Of Photovoltaics: Fundamentals And Applications* Elsevier, Amsterdam, **2003**.
[29] M. Remec, Š. Tomšič, M. Khenkin, Q. Emery, J. Li, F. Scheler, B. Glažar, M. Jankovec, M. Jošt, E. Unger, S. Albrecht, R. Schlatmann, B. Lipovšek, C. Ulbrich, M. Topič., *Adv. Energy Mater.*, **2024**, *14*, 2304452, https://doi.org/10.1002/aenm.202304452.

[30] "High-Throughput Aging System for Parallel Maximum Power Point Tracking of Perovskite Solar Cells - Köbler - 2022 - Energy Technology - Wiley Online Library." (Accessed: Aug, 2024). [Online]. Available: https://onlinelibrary.wiley.com/doi/full/10.1002/ente.202200234.
[31] G. A. Farias-Basulto, C. Ulbrich, R. Schlatmann, R. Klenk, *Jpn. J. Appl. Phys.* **2023**, *62*, SK1023.
[32] G. A. Farias-Basulto, P. Reyes-Figueroa, M. Aghaei, C. Ulbrich, B. Szyszka, R. Schlatmann, R. Klenk, 36th EU PVSEC, 1141–45. Marseille, France, **2019**, https://doi.org/10.4229/EUPVSEC20192019-4AV.2.12.
[33] G. A. Farias-Basulto, P. Reyes-Figueroa, C. Ulbrich, B. Szyszka, R. Schlatmann, R. Klenk, *Solar Energy* **2020**, *208*, 859.
[34] M. Gostein, L. Dunn, in *37th IEEE Photovoltaic Specialists Conf.* Jun. **2011**, pp. 003126–003131, https://doi.org/10.1109/PVSC.2011.6186605.
[35] J. Chantana, T. Kato, H. Sugimoto, T. Minemoto, *Progress in Photovoltaics: Research and Applications* **2018**, *26*, 868.
[36] T. Kobayashi, H. Yamaguchi, T. Nakada, *Prog. Photovolt: Res. Appl.* **2014**, *22*, 115.
[37] B. Li, M. Lin, C. Kan, P. Hang, Y. Yao, Z. Hu, Y. Wang, Y. Zhang, W. Zhong, D. Yang, X. Yu, *Solar RRL* **2022**, *6*, 2200050.
[38] X. Deng, X. Wen, J. Zheng, T. Young, C. F. J. Lau, J. Kim, M. Green, S. Huang, A. Ho-Baillie, *Nano Energy* **2018**, *46*, 356.
[39] J. Peng, Y. Sun, Y. Chen, Y. Yao, Z. Liang, *ACS Energy Lett.* **2016**, *1*, 1000.
[40] J. Herterich, M. Unmüssig, G. Loukeris, M. Kohlstädt, U. Würfel, *Energy Technol.* **2021**, *9*, 2001104.
[41] H. Tsai, R. Asadpour, J. Blancon, C. C. Stoumpos, O. Durand, J. W. Strzalka, B. Chen, R. Verduzco, P. M. Ajayan, S. Tretiak, J. Even, M. A. Alam, M. G. Kanatzidis, W. Nie, A. D. Mohite, *Science* **2018**, *360*, 67.
[42] X. Wu, X. Wu, J. Ma, M. Qin, X. Guo, Y. Li, Z. Qin, J. Xu, X. Lu, *Adv. Funct. Mater.* **2021**, *31*, 2101287.
[43] X. Zhang, S.-H. Wei, *Phys. Rev. Lett.* **2022**, *128*, 136401.
[44] E. Mosconi, D. Meggiolaro, H. J. Snaith, S. D. Stranks, F. D. Angelis, *Energy Environ. Sci.* **2016**, *9*, 3180.
[45] J. Wang, X. Duan, W.-J. Yin, *J. Phys. Chem. Lett.* **2021**, *12*, 9328.
[46] B. Cai, B. Cai, X. Yang, Z. Yu, Y. Liang, Y. Shan, A. Hagfeldt, L. Sun, *J. Power Sources* **2020**, *472*, 228506.
[47] G. A. Farias-Basulto, I. Kafedjiska, T. Bertram, M. Riedel, Q. Emery, M. Remec, P. Graniero, M. Khenkin, C. A. Kaufmann, I. Lauermann, R. Klenk, R. Schlatmann, C. Ulbrich, *HZB Data Service* **2025**, https://doi.org/10.5442/ND000012.
[48] B. Roose, *RSC Adv.* **2021**, *11*, 12095.
[49] M. Khenkin, M. Khenkin, H. Köbler, M. Remec, R. Roy, U. Erdil, J. Li, N. Phung, G. Adwan, G. Paramasivam, Q. Emery, E. Unger, R. Schlatmann, C. Ulbrich, A. Abate, *Energy Environ. Sci.* **2024**, *17*, 602.
[50] G. A. Farias-Basulto, M. Riedel, M. Khenkin, R. Schlatmann, R. Klenk, C. Ulbrich, *Data Brief.* **2023**, *48*, 109273.
[51] G. A. Farias-Basulto, M. Á. Sevillano-Bendezú, M. Riedel, M. Khenkin, J. A. Töfflinger, R. Schlatmann, R. Klenk, C. Ulbrich, *Solar Energy* **2023**, *266*, 112175.
[52] U. Rau, H. W. Schock, *Appl. Phys. A: Mater. Sci. Process.* **1999**, *69*, 131.
[53] M. A. Green, *Solar Cells - Operating Principles, Technology And System Applications*, The University of New South Wales, New South Wales, **1998**.
[54] A. Virtuani, E. Lotter, M. Powalla, *Thin Solid Films* **2003**, *431–432*, 443.
[55] S. Baumann, G. E. Eperon, A. Virtuani, Q. Jeangros, D. B. Kern, D. Barrit, J. Schall, W. Nie, G. Oreski, M. Khenkin, C. Ulbrich, R. Peibst, J. S. Stein, M. Köntges, *Energy Environ. Sci.* **2024**, 20, https://doi.org/10.1039/D4EE01898B.
[56] L. Duan, D. Walter, N. Chang, J. Bullock, D. Kang, S. P. Phang, K. Weber, T. White, D. Macdonald, K. Catchpole, H. Shen, *Nat Rev Mater* **2023**, *8*, 261.
[57] U. Erdil, M. Khenkin, W. M. B. de Araujo, Q. Emery, I. Lauermann, V. Paraskeva, M. Norton, S. Vediappan, D. K. Kumar, R. K. Gupta, I. Visoly-Fisher, M. Hadjipanayi, G. E. Georghiou, R. Schlatmann, A. Abate, E. A. Katz, C. Ulbrich, *Energy Technol.* **2025**, *13*, 2401280.
[58] D. L. King, J. A. Kratochvil, W. E. Boyson, *in Conf. Record of the Twenty Sixth IEEE Photovoltaic Specialists Conf. - 1997*, Anaheim, CA, USA: IEEE **1997**, 1183–1186, https://doi.org/10.1109/PVSC.1997.654300.